International Journal of Solids and Structures 48 (2011) 3099–3111

Contents lists available at ScienceDirect

International Journal of Solids and Structures

journal homepage: www.elsevier.com/locate/ijsolstr

Prediction of the initial thickness of shear band localization based on a reduced strain gradient theory

Shaohua Chen *, Biao Feng, Yueguang Wei, Tzuchiang Wang *

LNM, Institute of Mechanics, Chinese Academy of Sciences, Beijing 100190, China

ARTICLE INFO

Article history:
Received 10 January 2011
Received in revised form 2 June 2011
Available online 23 July 2011

Keywords:
Shear band localization
Thickness
Tilt angle
Strain gradient theory

ABSTRACT

Plastic flow localization in ductile materials subjected to pure shear loading and uniaxial tension is investigated respectively in this paper using a reduced strain gradient theory, which consists of the couple-stress (CS) strain gradient theory proposed by Fleck and Hutchinson (1993) and the strain gradient hardening (softening) law (C–W) proposed by Chen and Wang (2000). Unlike the classical plasticity framework, the initial thickness of the shear band and the strain rate distribution in both cases are predicted analytically using a bifurcation analysis. It shows that the strain rate is obviously non-uniform inside the shear band and reaches a maximum at the center of the shear band. The initial thickness of the shear band depends on not only the material intrinsic length l_{cs} but also the material constants, such as the yield strength, ultimate tension strength, the linear hardening and softening shear moduli. Specially, in the uniaxial tension case, the most possible tilt angle of shear band localization is consistent qualitatively with the existing experimental observations. The results in this paper should be useful for engineers to predict the details of material failures due to plastic flow localization.

1. Introduction

Plenty of experiments have shown that metallic material behaviors display strong size effects when the characteristic length scale is on the order of micrometer or sub-micrometer (Yang et al., 1990; Stelmashenko et al., 1993; Fleck et al., 1994; Lloyd, 1994; Atkinson, 1995; Ma and Clarke, 1995; McElhaney et al., 1998; Stolken and Evans, 1998; Saha et al., 2001; Saha and Nix, 2002; Swadener et al., 2002; Feng and Nix, 2004; Chen et al., 2005). For examples, Fleck et al. (1994) found that the torsion strength of a thin copper wire increases about three times when the diameter of thin copper wire decreases from 170 μm to 12 μm. Stolken and Evans (1998) found that the bending strength of a thin nickel beam with thickness at the micrometer scale increases significantly along with a decreasing thickness of the ultra-thin beam. Lloyd (1994) observed that the flow strength of aluminum-magnesium matrix composites reinforced by silicon-carbide particles increases substantially as the particle diameter is reduced from 16 μm to 7.5 μm at a fixed particle volume fraction of 15%.

The classical plasticity theory can not predict these size effects due to no intrinsic lengths included in the constitutive model. Strain gradient theories have been developed to extend continuum plasticity to the micrometer scale, which can be divided into two classes. The first one involves the higher-order stress as the work conjugate of the strain gradient. In these higher-order strain gradient theories, the order of the equilibrium equations are higher than that in the conventional continuum theories, therefore additional boundary conditions are required. Examples include Fleck and Hutchinson (1993, 1997, 2001), Fleck et al. (1994), Fleck and Willis (2009), Gao et al. (1999a,b), Gurtin (2000, 2002), Huang et al. (2000a,b), Hwang et al. (2003, 2002), Lam et al. (2003), Yang et al. (2002), Yi et al. (2009). Another framework of strain gradient plasticity theories does not involve higher-order stress and requires no additional boundary conditions. The plastic strain gradient comes into play through the incremental plastic modulus. Examples include Bassani and Acharya (1995), Acharya and Beaudoin (2000), Chen and Wang (2000, 2001, 2002a), Bassani (2001), Evers et al. (2002), Huang et al. (2004), Hu et al. (2005), et al.

Strain gradient plasticity theories have given reasonable agreements with the size dependence in several typical experiments, such as thin-wire torsion (e.g. Chen and Wang, 2000, 2001, 2002a; Fleck et al., 1994; Gao and Huang, 2001), thin-beam bending (e.g. Chen and Wang, 2000, 2001, 2002a; Gao and Huang, 2001; Stolken and Evans, 1998), micro- and nano-indentation (e.g. Chen et al., 2004; Huang et al., 2000b; Nix and Gao, 1998; Saha et al., 2001; Wei and Hutchinson, 2003; Xue et al., 2002) as well as the composite material experiments (e.g. Chen and Wang, 2002b; Fleck and Hutchinson, 1997; Shu and Fleck, 1999; Wei, 2001; Liu and Hu, 2005).

* Corresponding authors. Tel.: +86 10 82543960; fax: +86 10 82543977 (S. Chen); tel.: +86 10 82543911; fax: +86 10 82543977 (T. Wang).
E-mail addresses: chenshaohua72@hotmail.com (S. Chen), tcwang@imech.ac.cn (T. Wang).

0020-7683/$ - see front matter © 2011 Elsevier Ltd. All rights reserved.
doi:10.1016/j.ijsolstr.2011.07.007

Classical plasticity theories also fail to explain the fracture behavior of some ductile materials. In 1994, Elssner et al. measured both the macroscopic fracture toughness and atomic work of separation of an interface between a single crystal of niobium and a sapphire single crystal. The macroscopic work of fracture was found to be two to three orders of magnitude higher than the atomic work of separation. This large difference between the macroscopic work of fracture and its counterpart at the atomic level was attributed to plastic dissipation in niobium, i.e., there must be significant plastic deformation associated with dislocation activities in niobium. However, Elssner et al. (1994) observed that the interface between two materials remained atomistically sharp. Meanwhile the stress level needed to produce atomic decohesion of a lattice or a strong interface is typically on the order of 0.03 times the Young's modulus, or 10 times the tensile yield stress. But the maximum stress level that can be achieved near a crack tip is not larger than 4 or 5 times the tensile yield stress of metals, according to models based on conventional plasticity theories (Hutchinson, 1997). This clearly falls short of triggering the atomic decohesion observed in Elssner et al.'s experiments (1994).

The strain gradient theories have also been successfully applied to study the crack tip field in order to narrow down the gap in the stress levels for macroscopic cracking and for atomistic fracture (Wei and Hutchinson, 1997; Jiang et al., 2001; Chen and Wang, 2002c; Mikkelsen and Goutianos, 2009). It is found that the stress fields ahead of a mode I crack tip consist of a strain gradient dominating field, a HRR field and an elastic K one with the distance far away from the crack tip. The effective stress in the strain gradient dominated field is improved significantly and achieves 10 times or more the tensile yield stress (Jiang et al., 2001; Chen and Wang, 2002c).

Shear band localization in metallic materials is another field that may involve length scales. However, due to the absence of material intrinsic length and neglect of the gradient terms, classical plasticity theories cannot predict the thickness of shear band. Moreover, in numerical simulation of localization, classical continuum models may frequently encounter such problems as spurious mesh-dependency and high sensitivity to constitutive relations.

Some strain gradient plasticity theories have been used to study the plastic flow localization. Aifantis (1984), Aifantis (1987), Zbib and Aifantis (1988), Zbib and Aifantis (1992) applied their gradient plasticity model to study shear band localization in metals. Fleck and Hutchinson (1998) and Zhao et al. (2005) predicted the shear band thickness in materials only with simple elastic and softening phases under pure shear loading. Shi et al. (2000) and Shi et al. (2009) studied the shear band localization using the deformation and flow version of MSG theory, respectively, but also with a pure shear model. Engelen et al. (2006) analyzed the ability of Fleck and Hutchinson (1997), Fleck and Hutchinson (2001) theories and the nonlocal theory of Engelen et al. (1999), Engelen et al. (2003) to handle material softening by considering the bifurcation of a bar under uniform tensile straining, in which they found that the Fleck and Hutchinson, 1997 theory showed the desired localization behavior at and beyond the transition from hardening to softening, while the pathological localization at the peak strength was not prevented by the Fleck and Hutchinson, 2001 theory and the non-uniform solutions could occur even before the peak load. As for the nonlocal theory of Engelen et al. (1999), Engelen et al. (2003), it allows for a transition from hardening to softening and within the softening regime it correctly predicts a localization band of finite width. Recently, a more systematical study on localization properties predicted by different gradient plasticity models has been done by Jirasek and Rolshoven (2009a), Jirasek and Rolshoven (2009b), in which they divided the gradient theories into two distinct groups: strain gradient models and models with gradients of internal variables. The evolution of localization in a one-dimensional setting that a bar of a constant cross section was fixed at one end and loaded by an applied displacement at the opposite end, was analyzed systematically. In the first group, Jirasek and Rolshoven (2009a) considered the strain gradient plasticity model proposed by Chambon et al. (1998), the one proposed by Fleck and Hutchinson (1997) and the mechanism-based strain gradient plasticity theory suggested by Gao et al. (1999a), Gao et al. (1999b). Detailed analysis of the onset of localization, considered as a bifurcation from a uniform state, has shown that the first two models act as proper localization limiters, preventing localization of plastic yielding into a set of zero measure and at the same time allowing localization into a process zone of a finite thickness. However, considering the subsequent evolution of localization, the plastic zone tends to expand over the entire specimen in the first model and the plastic zone shrinks at late stage of softening and an instability develops in the second model. In the second group (Jirasek and Rolshoven, 2009b), models with gradients of internal variables are further divided into the one with gradient of internal variables appearing directly in the hardening-softening law and the one with implicit formulations. The same one-dimensional setting as that in Jirasek and Rolshoven (2009a) was analyzed and the reasonability of the initial bifurcation from a uniform state and response at late stages of the softening process was also mainly focused and discussed.

All of the above theoretical models are studied using the strain gradient plasticity theories, which have their own application range, i.e., the metallic materials, because most of the strain gradient theories are physically motivated by the concept of statistically store and geometrically necessary dislocations. Plastic localization in metallic materials may be analyzed by most of the strain gradient plasticity theories.

Shear bands can also present for metallic glass, polymers and geomaterials, and has attracted many researchers' interest, which are generally treated as material instabilities by bifurcation theory (Hadamad, 1903; Hill, 1958; Thomas, 1961; Rudnicki and Rice, 1975; Rice, 1976; Peirce et al., 1983; Ortiz, 1987; Ottosen and Runesson, 1991; De Borst and Van der Giessen, 1998). Based on the earlier experiments (Oda et al., 1982), Oda and Kazama (1998) found that the formation of shear bands coincides with the buckling of the particle columns through particle rotation rather than sliding. Particle rotation in the shear band is unidirectional and highly non-uniform (see, Gardiner and Tordesillas, 2004). In this circumstance, the rotation gradient terms become very important and can no longer be neglected. Oda and Iwashita (2000) proved that the presence of the small couple stress plays a very important role in the formation and development of microstructure in shear bands based on numerical simulation and laboratory tests. However, theoretical analysis for the formation and thickness of shear band localization considering the function of the couple-stress is absence. Furthermore, uniaxial tension or compression tests are often used to study the shear bands in addition to the pure shear tests. Peirce et al. (1983) considered the strain hardening properties and crystal geometries to analyze the direction of shear band formation for single crystals subjected to tensile loading. Ortiz (1987) presented a theoretical framework for the analysis of shear localized failure under biaxial and uniaxial stress loadings. Due to the absence of material length scale and neglect of the gradient terms, the thickness of shear bands can not be predicted. As for the inclination angle of shear bands in a uniaxial test, Schuster et al. (2007), Schuster et al. (2008), Donovan (1988), Donovan (1989) found that the tilt angle of the shear band is about 42°, independent of specimen size. Volkert et al. (2008) found the tilt angle is about $50 \pm 4^\circ$ in amorphous metals.

Inspired by the above experiments for metallic and non-metallic materials and the couple stress gradient theory considering rotation vectors with the assumption that crystalline-metallic

solids can be looked as materials composed by multi-crystals (Fleck and Hutchinson, 1993; Chen and Wang, 2001), obvious questions are as follows:

(1) Does the rotation gradient term become very important in predicting the thickness of plasticity flow localization for metallic materials, similar to the case for a granular one (Oda and Iwashita, 2000)?
(2) What factors will influence the tilt angle of shear band?
(3) Do the tilt angle or material constants influence the thickness of shear band?
(4) Is there a range of tilt angle for possible plastic flow localization?

In order to answer the above questions, a reduced strain gradient theory will be used to analyze plastic flow localization under pure shear loading and uniaxial tension one, respectively. Especially, the possible tilt angle of the shear band under uniaxial tension loading will be investigated theoretically.

One should be noted that the strain gradient theories belong to the framework of continuum mechanics, which do not focus on the specific microstructures and the microscopic mechanisms. All the materials analyzed by the strain gradient theories are assumed to be isotropic continuum one. The details of microstructure evolution are reflected by the intrinsic materials l_{cs} and l_1 corresponding to the rotation gradient and stretch gradient, respectively. The macroscopically observed materials' behaviors, as a manifestation of microscopic mechanism, are described by the constitutive law of materials.

2. Brief introduction of the reduced strain gradient theory

The strain gradient theory by Chen and Wang (2001), Chen and Wang (2002a) includes a general couple stress strain gradient theory, in which the effect of rotation gradient is considered through the interaction of the Cauchy stress and the couple stress, and an incremental hardening (softening) law, in which the stretch gradient, as an internal variable, influences the instantaneous hardening (softening) tangential moduli in order to avoid higher order stress. The reduced strain gradient theory in this paper comes from the strain gradient theory by Chen and Wang (2001), Chen and Wang (2002a), in which we let the micro-rotation vector to be equal to the material rotation one and the general couple stress theory in Chen and Wang (2001), Chen and Wang (2002a) reduces to the CS strain gradient theory. The reduced strain gradient theory is now combined essentially by the couple stress strain gradient theory proposed by Fleck and Hutchinson (1993) and the strain gradient hardening (softening) law suggested by Chen and Wang (2000).

The couple stress strain gradient theory (CS) proposed by Fleck and Hutchinson (1993) fits neatly within the framework of Toupin (1962), Mindlin (1964), Mindlin (1965) and Eringen (1968), which are based on the general couple stress theory developed by Cosserat and Cosserat (1909). In CS theory, it is assumed that the strain energy density of a homogeneous isotropic solid depends upon the scalar invariants of the strain tensor ε and the curvature tensor χ. The generalized (overall) effective stress Σ_e is defined as the work conjugate of the generalized (overall) effective strain E_e, and is a unique function of E_e. For an incompressible solid, the virtual work done on the solid per unit volume equals the increment in strain energy density

$$\delta w = \Sigma_e \delta E_e = \boldsymbol{\sigma} : \delta \boldsymbol{\varepsilon} + \boldsymbol{m} : \delta \boldsymbol{\chi} = \boldsymbol{s} : \delta \boldsymbol{\varepsilon} + \boldsymbol{m} : \delta \boldsymbol{\chi} \tag{1}$$

where

$$E_e^2 = \varepsilon_e^2 + l_{cs}^2 \chi_e^2 \quad \varepsilon_e^2 = \frac{2}{3}\varepsilon_{ij}\varepsilon_{ij} \quad \varepsilon_{ij} = \frac{1}{2}(u_{i,j} + u_{j,i}) \tag{2}$$

l_{cs} is an intrinsic material length associated with the rotation gradient. $\mathbf{s}$ is the deviatoric part of $\boldsymbol{\sigma}$. Micro-rotation vector $\boldsymbol{\omega}$, the rotation gradient tensor χ and the effective rotation gradient are defined as

$$\omega_i = \frac{1}{2} e_{ijk} u_{k,j} \quad \chi_{ij} = e_{its}\varepsilon_{js,t} \quad \chi_e^2 = \frac{2}{3}\chi_{ij}\chi_{ij} \tag{3}$$

Then the deviatoric stress tensor $\mathbf{s}$, couple stress tensor $\boldsymbol{m}$ can be obtained as

$$s_{ij} = \frac{\partial w}{\partial \varepsilon_{ij}} = \frac{2}{3}\frac{\Sigma_e}{E_e}\varepsilon_{ij} \quad m_{ij} = \frac{\partial w}{\partial \chi_{ij}} = \frac{2}{3}\frac{\Sigma_e}{E_e} l_{cs}^2 \chi_{ij} \tag{4}$$

where

$$\Sigma_e = \left(\sigma_e^2 + l_{cs}^{-2} m_e^2\right)^{1/2} \quad \sigma_e^2 = \frac{3}{2} s_{ij} s_{ij} \quad m_e^2 = \frac{3}{2} m_{ij} m_{ij} \tag{5}$$

The classical plasticity hardening (softening) law is expressed as

$$\sigma_e = A(\varepsilon_e) \tag{6}$$

In order to consider the influence of stretch gradient, an incrementally hardening or softening law proposed by Chen and Wang (2000) is introduced

$$\dot{\Sigma}_e = A'(E_e)\left(1 + \frac{l_1\eta_1}{E_e}\right)^{1/2} \dot{E}_e = B(E_e, l_1\eta_1)\dot{E}_e \tag{7}$$

where $B(E_e, l_1\eta_1)$ is a new function including the stretch gradient effect. l_1 is an intrinsic material length associated with the stretch gradient and η_1 is the effective stretch gradient defined as $\eta_1 = \sqrt{\eta_{ijk}^{(1)}\eta_{ijk}^{(1)}}$. The definition of $\eta_{ijk}^{(1)}$ can be found in Smyshlyaev and Fleck (1996). Due to the incremental law, no high-order stress is introduced in the reduced strain gradient theory, only the Cauchy stress tensor and the couple stress one. The equilibrium equations can be written as (Fleck and Hutchinson, 1993)

$$\sigma_{ij,j} + \tau_{ij,j} = 0 \tag{8}$$

where τ_{ij} is the anti-symmetric part of the Cauchy stress and can be given as

$$\tau_{jk} = \frac{1}{2} e_{ijk} m_{ip,p} \tag{9}$$

The traction boundary conditions are the same as those in Fleck and Hutchinson (1993),

$$\begin{cases} \mathbf{T} = (\boldsymbol{\sigma} + \boldsymbol{\tau}) \cdot \mathbf{n} \\ \mathbf{q} = \mathbf{m} \cdot \mathbf{n} \end{cases} \tag{10}$$

3. Plastic flow localization under pure shear

The simple model as shown in Fig. 1 has been adopted by Fleck and Hutchinson (1998), Shi et al. (2000), Zhao et al. (2005), Osinov and Wu (2009) and Shi et al. (2009) to study plastic flow localization using different strain gradient theories, in which the infinite solid is subjected to a remote pure shear loading σ_{21}^{∞}. Another simple setting that a bar of a constant cross section is fixed at one end and loaded by an applied displacement at the opposite end, has already been analyzed systematically by Jirasek and Rolshoven (2009a,b), which will not be investigated in the present paper.

Similar to Shi et al. (2009), a simple uniaxial stress-strain relation that exhibits the elastic, linear work hardening and softening behavior is adopted in the present paper as shown in Fig. 2. The elastic modulus is denoted as E, the linear work hardening modulus is E_t and the softening modulus is $-E_s$. The yield stress is σ_y and the ultimate tensile strength is σ_u.

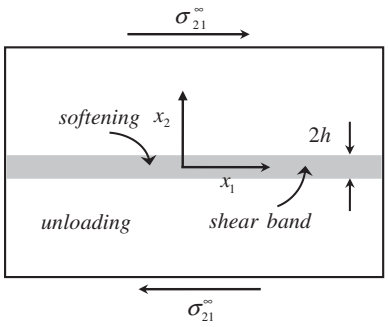

Fig. 1. Model of an infinite solid subjected to a remote pure shear σ_{21}^{∞} to study plastic flow localization. A shear band initiates parallel to the remote shear due to the material softening and elastic unloading happens outside the shear band. $2h$ is the thickness of shear band.

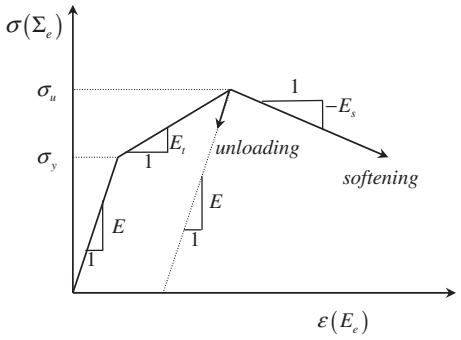

Fig. 2. Uniaxial stress-strain relation with Young's modulus E, linear hardening modulus E_t, yield stress σ_y, and the ultimate tensile strength σ_u. At the initiation of shear band, two strain paths at σ_u will happen, one (dashed line) corresponds to elastic unloading with modulus E, and the other (solid line) corresponds to softening with softening modulus $-E_s$ ($E_s < 0$).

The infinite solid is assumed to be incompressible so that the relation between the generalized effective stress Σ_e and the generalized effective strain E_e can be written as

$$\begin{cases} \Sigma_e = 3GE_e & \text{for } 0 \leqslant E_e \leqslant \frac{\sigma_y}{3G} \\ \Sigma_e = \sigma_y + 3G_t\left(E_e - \frac{\sigma_y}{3G}\right) & \text{for } \frac{\sigma_y}{3G} \leqslant E_e \leqslant \frac{\sigma_y}{3G} + \frac{\sigma_u - \sigma_y}{3G_t} \\ \Sigma_e = \sigma_u + 3G_s\left(E_e - \frac{\sigma_y}{3G} - \frac{\sigma_u - \sigma_y}{3G_t}\right) & \text{for } E_e \geqslant \frac{\sigma_y}{3G} + \frac{\sigma_u - \sigma_y}{3G_t} \end{cases} \tag{11}$$

where G, G_t and G_s are shear moduli corresponding to $E/3$, $E_t/3$ and $E_s/3$. The strain field inside the solid keeps uniform until the remote shear loading σ_{21}^{∞} reaches the maximum value $\sigma_u/\sqrt{3}$, which corresponds to the ultimate tensile strength σ_u in Fig. 2. At $\sigma_{21}^{\infty} = \sigma_u/\sqrt{3}$, there are two possible strain paths as shown in Fig. 2. One corresponds to the elastic unloading (dashed line) with a decreasing strain. The other corresponds to softening (solid line) with an increasing strain. In this model, the localized softening region is assumed as a band parallel to the remote shear loading as shown in Fig. 1.

Elastic unloading from the point at the ultimate tensile strength can be expressed as

$$\Sigma_e = \sigma_u + 3G\left(E_e - \frac{\sigma_y}{3G} - \frac{\sigma_u - \sigma_y}{3G_t}\right) \tag{12}$$

The nonvanishing displacement in the present model is assumed to be u_1, which is parallel to the direction of the external pure shear σ_{21}^{∞} and depends only on the coordinate x_2 normal to the shear band as shown in Fig. 1. The non-zero strain rate and rotation gradient rate are

$$\dot{\varepsilon}_{12} = \dot{\varepsilon}_{21} = \frac{\dot{\gamma}}{2} \quad \dot{\chi}_{32} = -\frac{\dot{\gamma}_{,2}}{2} \tag{13}$$

where $\gamma = du_1/dx_2$ is the engineering shear strain and is also a function of the coordinate x_2.

The rate of the generalized effective strain is given as

$$\dot{E}_e = \frac{\dot{\gamma}}{\sqrt{3}} \tag{14}$$

Considering the constitutive Eq. (4) and the non-zero rotation gradient rate $\dot{\chi}_{32}$, one can see that the non-zero couple stress rate is only $\dot{m}_{32}$. Then, the nonvanishing rate of anti-symmetric part of Cauchy stress is

$$\dot{\tau}_{12} = -\dot{\tau}_{21} = \frac{\dot{m}_{32,2}}{2} \tag{15}$$

The couple stress m_{ij} and the anti-symmetric part of Cauchy stress τ_{ij} also depend only on the coordinate x_2, then the equilibrium equation can be written as

$$\sigma_{12,2} + \tau_{12,2} = 0 \tag{16}$$

which can be integrated and written as an incremental form

$$\dot{\sigma}_{12} + \dot{\tau}_{12} = \dot{\sigma}_{21}^{\infty} \tag{17}$$

3.1. Bifurcation analysis outside the shear band

At the point of ultimate tensile strength, bifurcation analysis is used to study the initiation of a shear band. One should note that at the moment of shear band initiating, the strain field is still uniform but the rate of strain field is non-uniform, i.e., $\eta_1 = 0$, $\dot{\eta}_1 \neq 0$, $\chi_e = 0$, $\dot{\chi}_e \neq 0$, which has also been adopted in Engelen et al. (2006), Jirasek and Rolshoven (2009a), Jirasek and Rolshoven (2009b), Shi et al. (2009).

The solid outside the shear band undergoes elastic unloading so that it abides by the relation describing in Eq. (12). The incremental relation between the rate of the generalized effective stress $\dot{\Sigma}_e$ and the rate of generalized effective strain E_e is

$$\dot{\Sigma}_e = 3G\dot{E}_e\left(1 + \frac{l_1\eta_1}{E_e}\right)^{1/2} \tag{18}$$

The rates of symmetric and anti-symmetric parts of Cauchy stress outside the shear band at the moment of shear band initiating, can be obtained from Eqs. (4) and (18) as

$$\begin{cases} \dot{\sigma}_{12} = \left(\frac{2}{3}\frac{\Sigma_e}{E_e}\varepsilon_{12}\right)^{\bullet} = G\dot{\gamma} \\ \dot{\tau}_{12} = \frac{1}{2}\dot{m}_{32,2} = \left[\left(\frac{1}{3}\frac{\Sigma_e}{E_e}l_{cs}^2\chi_{32}\right)_{,2}\right]^{\bullet} = -\frac{\sigma_u}{6\varepsilon_u}l_{cs}^2\dot{\gamma}_{,22} \end{cases} \tag{19}$$

where

$$\varepsilon_u = \frac{\sigma_y}{3G} + \frac{\sigma_u - \sigma_y}{3G_t}.$$

From above, one should note that there is no influence of the stretch gradient length scale l_1 on the behavior of materials outside the initial shear band since we have $\eta_1 = 0$.

Substituting Eq. (19) into equilibrium Eq. (17) yields the governing equation outside the shear band

$$G\dot{\gamma} - \frac{\sigma_u}{6\varepsilon_u}l_{cs}^2\dot{\gamma}_{,22} = \dot{\sigma}_{21}^{\infty} \tag{20}$$

The solution to the above differential equation is

$$\begin{cases} \dot{\gamma} = \frac{\dot{\sigma}_{12}^{\infty}}{G} + Ae^{-\xi x_2} + Be^{\xi x_2} \\ \xi = \sqrt{\frac{6\varepsilon_u G}{\sigma_u l_{cs}^2}} = \frac{1}{l_{cs}}\sqrt{\frac{2[G_t\sigma_y + G(\sigma_u - \sigma_y)]}{G_t\sigma_u}} \end{cases} \tag{21}$$

Due to anti-symmetry, we only consider the upper half-plane, namely $x_2 \geqslant 0$. Then $x_2 \to +\infty$ yields a vanishing B.

Furthermore, we know that $\dot{\gamma} \leqslant 0$ outside the shear band and $\dot{\gamma} \geqslant 0$ inside the shear band. The continuity condition of $\dot{\gamma}$ across the shear band boundary requires

$$\dot{\gamma}|_{x_2=h} = 0 \tag{22}$$

which leads to

$$A = \frac{-\dot{\sigma}_{21}^{\infty} e^{\xi h}}{G} \tag{23}$$

3.2. Bifurcation analysis inside the shear band

When the shear band initiates, the tangent modulus changes discontinuously from a positive value G_t to a negative value G_s. The solid in the shear band undergoes softening and the relation between the overall effective stress and the overall effective strain can be expressed as

$$\Sigma_e = \sigma_u + 3G_s(E_e - \varepsilon_u) \quad (G_s < 0) \tag{24}$$

The incremental softening law with the effect of stretch gradient can be written as,

$$\dot{\Sigma}_e = 3G_s\dot{E}_e\left(1 + \frac{l_1\eta_1}{E_e}\right)^{1/2} \tag{25}$$

The rates of symmetric and anti-symmetric parts of Cauchy stress inside the shear band at the moment of shear band initiating, can be obtained from Eqs (4) and (25) as

$$\begin{cases} \dot{\sigma}_{21} = \left(\frac{2}{3}\frac{\Sigma_e}{E_e}\varepsilon_{21}\right)^{\bullet} = G_s\dot{\gamma} \\ \dot{\tau}_{12} = \frac{1}{2}\dot{m}_{32,2} = \left[\left(\frac{1}{3}\frac{\Sigma_e}{E_e}l_{cs}^2\chi_{32}\right)_{,2}\right]^{\bullet} = -\frac{\sigma_u}{6\varepsilon_u}l_{cs}^2\dot{\gamma}_{,22} \end{cases} \tag{26}$$

Substituting Eq. (26) into equilibrium Eq. (17) yields the governing equation inside shear band,

$$G_s\dot{\gamma} - \frac{\sigma_u}{6\varepsilon_u}l_{cs}^2\dot{\gamma}_{,22} = \dot{\sigma}_{21}^{\infty} \tag{27}$$

Also, the stretch gradient has no effect on the behavior of materials inside the initial shear band. Only the rotation gradient works at the moment of shear band initiating.

The solution to the above differential Eq. (27) can be obtained,

$$\begin{cases} \dot{\gamma} = \frac{\dot{\sigma}_{21}^{\infty}}{G_s} + C\sin(\eta x_2) + D\cos(\eta x_2) \\ \eta = \sqrt{-\frac{6\varepsilon_u G_s}{\sigma_u l_{cs}^2}} = \frac{1}{l_{cs}}\sqrt{\frac{2[G_s G_t\sigma_y + GG_s(\sigma_u - \sigma_y)]}{-GG_t\sigma_u}} \end{cases} \tag{28}$$

The anti-symmetric condition about the center of shear band requires

$$\dot{\gamma}_{,2}|_{x_2=0} = 0 \tag{29}$$

which also suggests that $\dot{\gamma}$ reaches maximum at the center of shear band. Then we find

$$C = 0 \tag{30}$$

At the boundary of shear band, the continuity of the shear strain rate $\dot{\gamma}$ requires

$$\dot{\gamma}|_{x_2=h-0} = \dot{\gamma}|_{x_2=h+0} \tag{31}$$

which results in

$$D = \frac{-\dot{\sigma}_{12}^{\infty}}{G_s\cos(\eta h)} \tag{32}$$

Then, the rate of shear strain in the upper half-plane can be expressed as

$$\begin{cases} \dot{\gamma} = \frac{\dot{\sigma}_{21}^{\infty}}{G}[1 - e^{\xi(h-x_2)}], & \text{at } x_2 > h \\ \dot{\gamma} = \frac{\dot{\sigma}_{21}^{\infty}}{G_s}\left[1 - \frac{\cos\eta x_2}{\cos\eta h}\right], & \text{at } 0 \leqslant x_2 \leqslant h \end{cases} \tag{33}$$

Furthermore, the continuity of couple stress traction at $x_2 = h$ requires

$$\dot{\gamma}_{,2}|_{x_2=h-0} = \dot{\gamma}_{,2}|_{x_2=h+0} \tag{34}$$

which yields the shear band thickness analytically as,

$$h = \frac{l_{cs}}{2}\sqrt{\frac{-2GG_t\sigma_u}{G_sG_t\sigma_y + GG_s(\sigma_u - \sigma_y)}}\left(\pi - \arctan\sqrt{\frac{-G_s}{G}}\right) \tag{35}$$

Here one can see that the initial thickness of shear band has a linear relation with the material intrinsic length l_{cs} and depends also on the material constants, such as the elastic shear modulus, the hardening tangential modulus, the softening one, the yield stress and the ultimate tensile strength.

The evolution of plasticity localization is out of scope of the present paper. Simply, according to Jirasek and Rolshoven (2009a), Jirasek and Rolshoven (2009b), the above solution remains valid if the rates are replaced by finite increments with respect to the state at bifurcation since the internal length l_{cs} is normally considered as a constant. The size and shape of the shear band therefore remain constant. As for a nonlinear softening law, methods used in Jirasek and Rolshoven (2009a), Jirasek and Rolshoven (2009b) should be required to analyze the evolution of plasticity localization.

4. Plastic flow localization under uniaxial tension

In contrast to Section 3, the characteristics of shear band localization under uniaxial tension is investigated in this section. The plane stress tension model is shown in Fig. 3, in which an infinite thin plate is subjected to a remote uniform stress σ^{∞}. The deformation inside the plate increases uniformly with the remote loading σ^{∞} until it reaches the ultimate tensile strength σ_u as shown in Fig. 2. After that, a shear band initiates with a tilt angle θ as shown in Fig. 3, outside which elastic unloading will happen and inside which material softening emerges simultaneously. Thus the strain field becomes nonuniform corresponding to a decreasing strain outside the shear band and an increasing strain inside the shear band, respectively. The solid in the uniaxial tension model is also assumed to abide by the simple uniaxial stress-strain relation in Eq. (11).

When the remote uniform stress σ^{∞} reaches the ultimate tensile stress σ_u, the stresses in the Cartesian coordinate system (x_1, x_2) as shown in Fig. 3 are obtained as

$$\sigma_{11} = \sigma_u\sin^2\theta \quad \sigma_{22} = \sigma_u\cos^2\theta \quad \sigma_{12} = \frac{1}{2}\sigma_u\sin(2\theta) \tag{36}$$

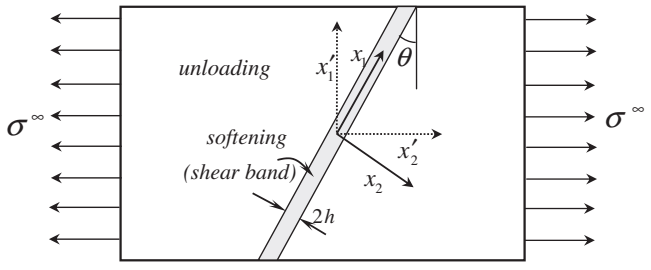

Fig. 3. Model of an infinite thin plate subjected to remote uniaxial tension to study plastic flow localization. A shear band will initiate at a tilt angle θ when σ^{∞} increases to the ultimate tensile strength σ_u. $2h$ is the thickness of shear band.

Then the strains can be expressed as

$$\begin{cases} \varepsilon_{11} = \varepsilon_u\left(\sin^2\theta - \frac{1}{2}\cos^2\theta\right) \\ \varepsilon_{22} = \varepsilon_u\left(\cos^2\theta - \frac{1}{2}\sin^2\theta\right) \\ \varepsilon_{33} = -(\varepsilon_{11}+\varepsilon_{22}) = -\frac{\varepsilon_u}{2} \\ \varepsilon_{12} = \frac{3\varepsilon_u \sin(2\theta)}{4} \end{cases} \tag{37}$$

where

$$\varepsilon_u = \frac{\sigma_y}{3G} + \frac{\sigma_u - \sigma_y}{3G_t} \tag{38}$$

If all the material undergoes an elastic unloading when the remote stress σ^∞ attains the ultimate tensile stress σ_u (actually, this case is not real), the displacement functions for the unloading line can be obtained as

$$\begin{cases} u_1' = -\frac{1}{2}\left(\frac{\sigma_y}{3G} + \frac{\sigma_u-\sigma_y}{3G_t} - \frac{\sigma_u}{3G} + \frac{\sigma^\infty}{3G}\right)x_1' \\ u_2' = \left(\frac{\sigma_y}{3G} + \frac{\sigma_u-\sigma_y}{3G_t} - \frac{\sigma_u}{3G} + \frac{\sigma^\infty}{3G}\right)x_2' \end{cases} \tag{39}$$

Using the formula of coordinate transformation, the displacement field in the coordinate systems (x_1,x_2) can be written as

$$\begin{cases} u_1 = \frac{1}{2}\left(\frac{\sigma_y}{3G} + \frac{\sigma_u-\sigma_y}{3G_t} - \frac{\sigma_u}{3G} + \frac{\sigma^\infty}{3G}\right)(3\sin^2\theta - 1)x_1 \\ \qquad + \frac{3}{4}\left(\frac{\sigma_y}{3G} + \frac{\sigma_u-\sigma_y}{3G_t} - \frac{\sigma_u}{3G} + \frac{\sigma^\infty}{3G}\right)\sin(2\theta)x_2 \\ u_2 = \frac{3}{4}\left(\frac{\sigma_y}{3G} + \frac{\sigma_u-\sigma_y}{3G_t} - \frac{\sigma_u}{3G} + \frac{\sigma^\infty}{3G}\right)\sin(2\theta)x_1 \\ \qquad + \frac{1}{2}\left(\frac{\sigma_y}{3G} + \frac{\sigma_u-\sigma_y}{3G_t} - \frac{\sigma_u}{3G} + \frac{\sigma^\infty}{3G}\right)(3\cos^2\theta - 1)x_2 \end{cases} \tag{40}$$

Then, the velocity field in the coordinate system (x_1,x_2) is given as

$$\begin{cases} v_1 = \frac{\dot\sigma^\infty}{6G}(3\sin^2\theta - 1)x_1 + \frac{\dot\sigma^\infty}{4G}\sin(2\theta)x_2 \\ v_2 = \frac{\dot\sigma^\infty}{4G}\sin(2\theta)x_1 + \frac{\dot\sigma^\infty}{6G}(3\cos^2\theta - 1)x_2 \end{cases} \tag{41}$$

However, when the remote tension stress σ^∞ reaches the ultimate tensile strength σ_u, two possible strain paths exist as shown in Fig. 2. One corresponds to the elastic unloading (dashed line) outside the shear band and the other corresponds to the softening (solid line) inside the shear band. On the other hand, the solid abides by the reduced strain gradient theory not the classical one. The generation of shear band and the strain gradient theory will cause a fluctuation on the velocity field derived from the classical plasticity theory in Eq. (41). We assume that the fluctuation on velocity field will only influence the term in the direction of x_2. Then, the velocity field governed by the reduced strain gradient theory in Section 2 can be written as

$$\begin{cases} v_1 = \frac{\dot\sigma^\infty}{6G}(3\sin^2\theta - 1)x_1 + k_1(x_2) \\ v_2 = \frac{\dot\sigma^\infty}{4G}\sin(2\theta)x_1 + k_2(x_2) \end{cases} \tag{42}$$

where $k_1(x_2)$ and $k_2(x_2)$ are two unknown functions about x_2.

Eq. (42) yields the known strain rate

$$\dot\varepsilon_{11} = \frac{\dot\sigma^\infty}{6G}(3\sin^2\theta - 1) \tag{43}$$

but $\dot\varepsilon_{22}$ and $\dot\varepsilon_{12}$ are still unknown. Although the field of strain rate is nonuniform when the shear band initiates, $\dot\varepsilon_{22}$ and $\dot\varepsilon_{12}$ should still be uniform a little outside the shear band.

The non-vanishing rate of rotation gradient is then obtained as

$$\boldsymbol{\dot\chi} = \begin{pmatrix} 0 & 0 & -\dot\varepsilon_{22,2} \\ 0 & 0 & 0 \\ 0 & -\dot\varepsilon_{12,2} & 0 \end{pmatrix} \tag{44}$$

and the rate of the overall effective strain can be written as

$$\dot E_e = \dot\varepsilon_{12}\sin(2\theta) + \dot\varepsilon_{11}\sin^2\theta + \dot\varepsilon_{22}\cos^2\theta \tag{45}$$

The non-vanishing rates of the couple stress and the anti-symmetric parts of Cauchy stress can be written respectively as

$$\boldsymbol{\dot m} = \begin{pmatrix} 0 & 0 & \dot m_{13} \\ 0 & 0 & 0 \\ 0 & \dot m_{32} & 0 \end{pmatrix} \quad \boldsymbol{\dot\tau} = \begin{pmatrix} 0 & \dot m_{32,2}/2 & 0 \\ -\dot m_{32,2}/2 & 0 & 0 \\ 0 & 0 & 0 \end{pmatrix} \tag{46}$$

which also depend only on x_2, such that the equilibrium equation can be simplified as

$$\begin{cases} \sigma_{12,2} + \tau_{12,2} = 0 \\ \sigma_{22,2} = 0 \end{cases} \tag{47}$$

Eq. (47) yields the incremental form

$$\begin{cases} \dot\sigma_{12} + \dot\tau_{12} = \frac{\dot\sigma^\infty}{2}\sin(2\theta) \\ \dot\sigma_{22} = \dot\sigma^\infty\cos^2\theta \end{cases} \tag{48}$$

which should govern both fields outside and inside the shear band.

4.1. Bifurcation analysis outside the shear band

At the moment of shear band initiating, the solid outside the shear band will undergo an elastic unloading. Then, the relation of the generalized effective stress Σ_e and the generalized effective strain E_e for the solid outside the shear band is

$$\Sigma_e = \sigma_u + 3G\left(E_e - \frac{\sigma_y}{3G} - \frac{\sigma_u - \sigma_y}{3G_t}\right) \tag{49}$$

Considering the effect of the stretch gradient yields

$$\dot\Sigma_e = 3G\dot E_e\left(1 + \frac{l_1\eta_1}{E_e}\right)^{1/2} \tag{50}$$

The rates of symmetric and anti-symmetric parts of Cauchy stress outside the shear band are

$$\begin{cases} \dot\sigma_{21} = \left(\frac{2\Sigma_e}{3E_e}\varepsilon_{21}\right)^\bullet = \left(\frac{2\sigma_u}{3\varepsilon_u} - \frac{\sin^2(2\theta)}{2}\frac{\sigma_u - 3G\varepsilon_u}{\varepsilon_u}\right)\dot\varepsilon_{21} \\ \qquad - \frac{\sin(2\theta)}{2}\frac{\sigma_u - 3G\varepsilon_u}{\varepsilon_u}(\dot\varepsilon_{11}\sin^2\theta + \dot\varepsilon_{22}\cos^2\theta) \\ \dot s_{22} = \left(\frac{2\Sigma_e}{3E_e}\varepsilon_{22}\right)^\bullet = \frac{2\sigma_u}{3\varepsilon_u}\dot\varepsilon_{22} - \frac{2\cos^2\theta - \sin^2\theta}{3}\frac{\sigma_u - 3G\varepsilon_u}{\varepsilon_u} \\ \qquad \times(\dot\varepsilon_{11}\sin^2\theta + \dot\varepsilon_{22}\cos^2\theta + \dot\varepsilon_{12}\sin(2\theta)) \\ \dot s_{33} = \left[\frac{-2\Sigma_e}{3E_e}(\varepsilon_{11} + \varepsilon_{22})\right]^\bullet = -\frac{2\sigma_u(\dot\varepsilon_{11} + \dot\varepsilon_{22})}{3\varepsilon_u} + \frac{\sigma_u - 3G\varepsilon_u}{3\varepsilon_u} \\ \qquad \times[\dot\varepsilon_{11}\sin^2\theta + \dot\varepsilon_{22}\cos^2\theta + \dot\varepsilon_{12}\sin(2\theta)] \\ \dot\tau_{12} = \frac{1}{2}\dot m_{32,2} = \left[\left(\frac{1}{3}\frac{\Sigma_e}{E_e}l_{cs}^2\chi_{32}\right)_{,2}\right]^\bullet = -\frac{\sigma_u}{3\varepsilon_u}l_{cs}^2\dot\varepsilon_{12,22} \end{cases} \tag{51}$$

Due to the plane stress state, it is reasonable to assume

$$\dot\sigma_{33} = 0 \tag{52}$$

Then, one can obtain

$$\begin{aligned} \dot\sigma_{22} = {} & \dot\varepsilon_{11}\left[\frac{2\sigma_u}{3\varepsilon_u} - \frac{1}{4}\frac{\sigma_u - 3G\varepsilon_u}{\varepsilon_u}\sin^2(2\theta)\right] \\ & + \dot\varepsilon_{22}\left[\frac{4\sigma_u}{3\varepsilon_u} - \frac{\sigma_u - 3G\varepsilon_u}{\varepsilon_u}\cos^4\theta\right] - \dot\varepsilon_{12}\frac{\sigma_u - 3G\varepsilon_u}{\varepsilon_u}\sin(2\theta)\cos^2\theta \end{aligned} \tag{53}$$

Substituting Eq. (53) into equilibrium Eq. (48) leads to the rate of ε_{22} as functions of $\dot\varepsilon_{11}$ and $\dot\varepsilon_{12}$,

$$\dot\varepsilon_{22} = \frac{\dot\sigma^\infty\cos^2\theta + \dot\varepsilon_{21}\frac{\sigma_u - 3G\varepsilon_u}{\varepsilon_u}\sin(2\theta)\cos^2\theta - \dot\varepsilon_{11}\left[\frac{2\sigma_u}{3\varepsilon_u} - \frac{\sigma_u - 3G\varepsilon_u}{4\varepsilon_u}\sin^2(2\theta)\right]}{\frac{4\sigma_u}{3\varepsilon_u} - \frac{\sigma_u - 3G\varepsilon_u}{\varepsilon_u}\cos^4\theta} \tag{54}$$

and the governing equation outside the shear band,

$$A_1\dot{\varepsilon}_{12}-\frac{\sigma_u}{3\varepsilon_u}l_{cs}^2\dot{\varepsilon}_{12,22}=B_1 \tag{55}$$

where the coefficients are

$$\begin{cases} A_1=\dfrac{2\sigma_u G_t G[3(\cos^4\theta+\sin^2(2\theta))(\sigma_u-\sigma_y)(G-G_t)+4\sigma_u G_t]}{[G_t\sigma_y+G(\sigma_u-\sigma_y)][3\cos^4\theta(\sigma_u-\sigma_y)(G-G_t)+4\sigma_u G_t]} \\ B_1=\dfrac{\dot{\sigma}^\infty G_t\sigma_u}{32}\dfrac{\left\{\begin{array}{l}\sigma_y(G-G_t)(9\sin(6\theta)-12\sin(4\theta)-51\sin(2\theta)) \\ +\sigma_u[\sin(2\theta)(51G+13G_t)-(9\sin(6\theta)-12\sin(4\theta))(G-G_t)]\end{array}\right\}}{[G_t\sigma_y+G(\sigma_u-\sigma_y)][3\cos^4\theta(\sigma_u-\sigma_y)(G-G_t)+4\sigma_u G_t]} \end{cases} \tag{56}$$

The solution to the above differential Eq. (55) is

$$\dot{\varepsilon}_{12}=\frac{B_1}{A_1}+Ae^{-\xi x_2}+Be^{\xi x_2} \tag{57}$$

where

$$\begin{cases} \frac{B_1}{A_1}=\frac{\dot{\sigma}^\infty\sin(2\theta)}{4G} \\ \xi=\sqrt{\frac{3\varepsilon_u A_1}{\sigma_u l_{cs}^2}} \end{cases} \tag{58}$$

Due to anti-symmetry, we only consider the upper half-plane, namely $x_2\geqslant 0$. When $x_2\to+\infty$, $\dot{\varepsilon}_{12}\to\dot{\sigma}^\infty\sin(2\theta)/(4G)$, which requires a vanishing B. On the other hand, the rate of the overall effective strain inside the shear band is positive and that outside the shear band is negative. On the boundary of the shear band, the continuity condition should be satisfied, i.e.,

$$\dot{E}_e|_{x_2=h}=0 \tag{59}$$

which gives

$$A=\frac{\dot{\sigma}^\infty}{e^{-\xi h}}\left[\begin{array}{l}\frac{1}{48G}\left(4\tan\theta-9\sin(2\theta)-12\sin^2\theta\tan\theta-\frac{6\sigma_y\cos^2\theta\cot\theta}{\sigma_u}-2\cot\theta\right) \\ +\frac{1}{8G_t}\left(\frac{\sigma_y\cot\theta\cos^2\theta}{\sigma_u}-\cos^2\theta\cot\theta\right)\end{array}\right] \tag{60}$$

4.2. Bifurcation analysis inside the shear band

Inside the shear band, the relation between the overall effective stress Σ_e and the overall effective strain E_e is

$$\Sigma_e=\sigma_u+3G_s(E_e-\varepsilon_u)\quad(G_s<0) \tag{61}$$

Considering the effect of stretch gradient yields

$$\dot{\Sigma}_e=3G_s\dot{E}_e\left(1+\frac{l_1\eta_1}{E_e}\right)^{1/2} \tag{62}$$

Then, the rates of symmetric and anti-symmetric parts of Cauchy stresses inside the shear band can be given,

$$\begin{cases} \dot{\sigma}_{21}=\left(\frac{2}{3}\frac{\Sigma_e}{E_e}\dot{\varepsilon}_{21}\right)^\bullet=\left(\frac{2\sigma_u}{3\varepsilon_u}-\frac{1}{2}\sin^2(2\theta)\frac{\sigma_u-3G_s\varepsilon_u}{\varepsilon_u}\right)\dot{\varepsilon}_{21} \\ \qquad -\frac{1}{2}\sin(2\theta)\frac{\sigma_u-3G_s\varepsilon_u}{\varepsilon_u}(\dot{\varepsilon}_{11}\sin^2\theta+\dot{\varepsilon}_{22}\cos^2\theta) \\ \dot{\sigma}_{22}=\dot{s}_{22}+\dot{\sigma}_m=\dot{\varepsilon}_{11}\left[\frac{2\sigma_u}{3\varepsilon_u}-\frac{\sigma_u-3G_s\varepsilon_u}{4\varepsilon_u}\sin^2(2\theta)\right]-\dot{\varepsilon}_{12}\frac{\sigma_u-3G_s\varepsilon_u}{\varepsilon_u}\sin(2\theta)\cos^2\theta \\ \qquad +\dot{\varepsilon}_{22}\left[\frac{4\sigma_u}{3\varepsilon_u}-\frac{\sigma_u-3G_s\varepsilon_u}{\varepsilon_u}\cos^4\theta\right] \\ \dot{\tau}_{12}=\frac{1}{2}\dot{m}_{32,2}=\left[\left(\frac{1}{3}\frac{\Sigma_e}{E_e}l_{cs}^2\chi_{32}\right)_{,2}\right]^\bullet=-\frac{\sigma_u}{3\varepsilon_u}l_{cs}^2\dot{\varepsilon}_{12,22} \end{cases} \tag{63}$$

Substituting the above stress rates into equilibrium Eq. (48) results in

$$\dot{\varepsilon}_{22}=\frac{\dot{\sigma}^\infty\cos^2\theta+\dot{\varepsilon}_{21}\frac{\sigma_u-3G_s\varepsilon_u}{\varepsilon_u}\sin(2\theta)\cos^2\theta-\dot{\varepsilon}_{11}\left[\frac{2\sigma_u}{3\varepsilon_u}-\frac{\sigma_u-3G_s\varepsilon_u}{4\varepsilon_u}\sin^2(2\theta)\right]}{\frac{4\sigma_u}{3\varepsilon_u}-\frac{\sigma_u-3G_s\varepsilon_u}{\varepsilon_u}\cos^4\theta} \tag{64}$$

and

$$A_2\dot{\varepsilon}_{12}-\frac{\sigma_u}{3\varepsilon_u}l_{cs}^2\dot{\varepsilon}_{12,22}=B_2 \tag{65}$$

where

$$\begin{cases} A_2=\dfrac{2\sigma_u G_t G\left\{\begin{array}{l}3\sigma_y G_s[(G_t-G)(\sin^2(2\theta)+\cos^4\theta)] \\ +G\sigma_u[3(\sin^2(2\theta)+\cos^4\theta)(G_s-G_t)+4G_t]\end{array}\right\}}{[G_t\sigma_y+G(\sigma_u-\sigma_y)][3(G_t-G)G_s\sigma_y\cos^4\theta+4GG_t\sigma_u+3G\sigma_u\cos^4\theta(G_s-G_t)]} \\ B_2=\dfrac{\dot{\sigma}^\infty G_t\sigma_u\left\{\begin{array}{l}\{-64G\sin(2\theta)+[9\sin(6\theta)+13\sin(2\theta) \\ -12\sin(4\theta)](G_s-G_t)\}G\sigma_u \\ +[-9G_s\sin(6\theta)+(64G-13G_s)\sin(2\theta) \\ +12G_s\sin(4\theta)](G-G_t)\sigma_y\end{array}\right\}}{-32[G_t\sigma_y+G(\sigma_u-\sigma_y)][3(G_t-G)G_s\sigma_y\cos^4\theta+4GG_t\sigma_u+3G\sigma_u\cos^4\theta(G_s-G_t)]} \end{cases} \tag{66}$$

(**a**) If the coefficient $A_2<0$, the solution to Eq. (65) is

$$\begin{cases} \dot{\varepsilon}_{12}=\frac{B_2}{A_2}+C\cos(\eta x_2)+D\sin(\eta x_2) \\ \eta=\sqrt{\frac{-3\varepsilon_u A_2}{\sigma_u l_{cs}^2}} \end{cases} \tag{67}$$

The anti-symmetry about the center of shear band requires

$$\dot{E}_{e,2}=0 \tag{68}$$

which also suggests that $\dot{E}_e$ reaches maximum at the center of shear band and results in

$$D=0 \tag{69}$$

The continuity of the rate of shear strain, $\dot{\varepsilon}_{12}$, at the boundary of the shear band requires

$$\dot{\varepsilon}_{12}|_{x_2=h-0}=\dot{\varepsilon}_{12}|_{x_2=h+0} \tag{70}$$

which gives

$$C=\left(\frac{B_1}{A_1}+Ae^{-\xi h}-\frac{B_2}{A_2}\right)\Big/\cos(\eta h) \tag{71}$$

The continuity of couple stress traction at the boundary of shear band requires

$$\dot{\varepsilon}_{12,2}|_{x_2=h-0}=\dot{\varepsilon}_{12,2}|_{x_2=h+0} \tag{72}$$

Then, we have,

$$\tan(\eta h)=\frac{\xi Ae^{-\xi h}}{\eta C\cos(\eta h)}=\sqrt{-\frac{A_1}{A_2}}\frac{Ae^{-\xi h}}{C\cos(\eta h)} \tag{73}$$

If we define the coefficient

$$\begin{aligned} A_3&=\frac{Ae^{-\xi h}}{C\cos(\eta h)} \\ &=-\frac{1}{2}\frac{[3(\cos\theta)^4(G_t-G)(\sigma_y-\sigma_u)+4G_t\sigma_u][G_t\sigma_y+G(\sigma_u-\sigma_y)]}{G\sigma_u G_t[3(3\cos^4\theta-4\cos^2\theta)(G_t-G)(\sigma_y-\sigma_u)-4G_t\sigma_u]}A_2 \end{aligned} \tag{74}$$

Due to $3(3\cos^4\theta-4\cos^2\theta)\in[-4,0]$ and $A_2<0$, the coefficient A_3 is always negative. The thickness of shear band is

$$h=\left[\pi+\arctan\left(\sqrt{-\frac{A_1}{A_2}}A_3\right)\right]/\eta \tag{75}$$

Then, the rates of shear strain inside and outside shear band at the moment of shear band initiating are,

$$\dot{\varepsilon}_{12}=\frac{\dot{\sigma}^\infty\sin(2\theta)}{4G}+Ae^{-\xi x_2}\quad\text{at } x_2>h \tag{76}$$

$$\dot{\varepsilon}_{12}=\frac{B_2}{A_2}+C\cos(\eta x_2)\quad\text{at } 0\leqslant x_2\leqslant h \tag{77}$$

where ξ and η are given in Eqs. (58) and (67), respectively.

(**b**) If the coefficient $A_2 > 0$, no reasonable solution can be found to Eq. (65). The solving procedure is very similar to the above analysis. Here we omit the details for conciseness.

From the above analysis, one can find that the coefficient A_2 depends on not only the material constants but also the tilt angle of shear band. In order to ensure a solution for the thickness of shear band, A_2 should be negative, which exerts some constraints on the tilt angle for a determined material. That means for one kind of material, the shear band can not initiate at an arbitrarily possible angle. There is a region of the tilt angle that shear band may initiate. Detail discussions will be carried out in the following numerical analysis.

5. Numerical results

Numerical analysis is studied in this section for further understanding the characteristics of shear band in pure shear and uniaxial tension models.

5.1. Plastic flow localization under pure shear

Eq. (33) could give the expression of the normalized shear strain rate inside and outside the shear band as

$$\begin{cases} \dfrac{G\dot{\gamma}}{|\dot{\sigma}_{21}^{\infty}|} = e^{\sqrt{\frac{G}{-G_s}}\left(\pi-\arctan\sqrt{\frac{-G_s}{G}}\right)\left(1-\frac{x_2}{h}\right)} - 1, & \text{at } x_2 > h \\ \dfrac{G\dot{\gamma}}{|\dot{\sigma}_{21}^{\infty}|} = \dfrac{G}{G_s}\left[\dfrac{\cos\left[\left(\pi-\arctan\sqrt{\frac{-G_s}{G}}\right)\frac{x_2}{h}\right]}{\cos\left(\pi-\arctan\sqrt{\frac{-G_s}{G}}\right)} - 1\right], & \text{at } 0 \leqslant x_2 \leqslant h \end{cases} \tag{78}$$

To investigate the nonuniform distribution of shear strain rate in the solid, we assume the softening secant modulus $G_s = -G/2$ where G is the elastic shear modulus. Fig. 4 shows the distribution of the shear strain rate normalized by the remote shear strain rate, $G\dot{\gamma}/|\dot{\sigma}_{21}^{\infty}|$, inside and outside the shear band. From Fig. 4, one can see that the shear strain rate increases monotonically from zero at the boundary of shear band to a maximum in the center. While the shear strain rate is uniform a little outside the shear band. The maximum shear strain rate normalized by the remote shear strain rate can be obtained from Eq. (78) as

$$\frac{G\dot{\gamma}_{max}}{|\dot{\sigma}_{21}^{\infty}|} = \frac{G}{G_s}\left[1/\cos\left(\pi - \arctan\sqrt{-G_s/G}\right) - 1\right] \tag{79}$$

which shows that the normalized maximum shear strain rate is independent of the yield stress σ_y, the ultimate tension strength σ_u, and the linear hardening secant modulus G_t. Only the ratio of $G/|G_s|$ shows influence on the maximum shear strain rate as shown in Fig. 5. One can see that the normalized maximum shear strain rate decreases along with an increasing ratio $|G_s|/G$, which displays a strong effect of the softening secant modulus on plastic flow localization. Specially, for $|G_s|/G = 0.1$, the maximum shear strain rate is more 20 times the remote shear strain rate, which shows a clear picture of plastic flow localization. It is well known that the counterpart predicted by the conventional plasticity theory will go from -1 outside the shear band to 2 inside the shear band.

The dimensionless thickness of shear band by the intrinsic length, h/l_{cs}, can be given from Eq. (35) as a function of material constants as

$$\frac{h}{l_{cs}} = \frac{\sqrt{2}}{2}\sqrt{\frac{G_t/G}{\frac{|G_s|}{G}\frac{G_t}{G}\frac{\sigma_y}{\sigma_u} + \frac{|G_s|}{G}\left(1-\frac{\sigma_y}{\sigma_u}\right)}}\left(\pi - \arctan\sqrt{\frac{|G_s|}{G}}\right) \tag{80}$$

Fig. 6 shows the variation of the dimensionless thickness of shear band along with the ratio $|G_s|/G$ for $G_t = G/2$ and different ratios σ_u/σ_y. From Fig. 6, one can see that the softening secant modulus has a significant effect on the dimensionless shear band thickness for fixed ratios G_t/G and σ_u/σ_y. With an increasing ratio of the ultimate tension strength σ_u to the yield stress σ_y, the dimensionless thickness of shear band decreases for fixed values G_t/G and $|G_s|/G$.

Fig. 7 shows the relation between the dimensionless thickness of shear band h/l_{cs} and the ratio G_t/G for a determined value $|G_s|/G = 1/2$ and different ratios σ_u/σ_y. As the ratio G_t/G increases from 0 to 1, the dimensionless thickness h/l_{cs} monotonously increases from 0 to a constant, which can also be found from Eq. (80) when $G_t/G = 1$. With an increasing σ_u/σ_y, the dimensionless thickness of shear band decreases slightly for fixed values G_t/G and $|G_s|/G$. Comparing Figs. 6 and 7 shows that the softening modulus has a more obvious effect on the plastic flow localization than the linear hardening one.

5.2. Plastic flow localization under uniaxial tension

The possible tilt angle of shear band in the case of uniaxial tension is constrained by the value of A_2 in Eq. (66). The dimensionless coefficient A_2 by the elastic shear modulus G can be expressed as

$$\frac{A_2}{G} = \frac{2\frac{G_t}{G}\left\{\begin{array}{l} 3\frac{\sigma_y}{\sigma_u}\frac{G_s}{G}\left[\left(\frac{G_t}{G}-1\right)\left(\sin^2(2\theta)+\cos^4\theta\right)\right] \\ +\left[3\left(\sin^2(2\theta)+\cos^4\theta\right)\left(\frac{G_s}{G}-\frac{G_t}{G}\right)+4\frac{G_t}{G}\right] \end{array}\right\}}{\left[\frac{G_t}{G}\frac{\sigma_y}{\sigma_u}+\left(1-\frac{\sigma_y}{\sigma_u}\right)\right]\left[3\left(\frac{G_t}{G}-1\right)\frac{G_s}{G}\frac{\sigma_y}{\sigma_u}\cos^4\theta+4\frac{G_t}{G}+3\cos^4\theta\left(\frac{G_s}{G}-\frac{G_t}{G}\right)\right]} \tag{81}$$

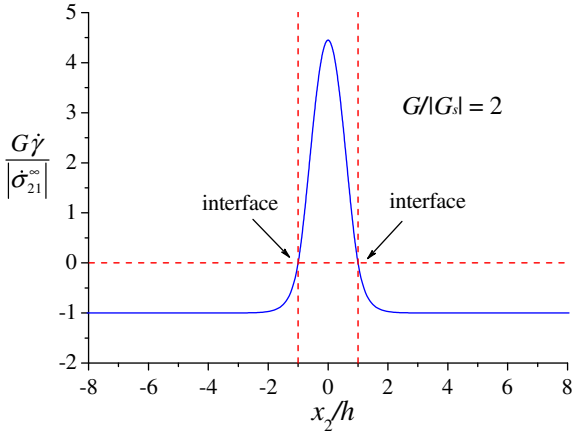

Fig. 4. The distribution of the normalized shear strain rate $G\dot{\gamma}/|\dot{\sigma}_{21}^{\infty}|$ inside and outside the shear band, where $\dot{\sigma}_{21}^{\infty}$ is the remote shear stress rate, G is the elastic shear modulus and the softening secant modulus $G_s = -G/2$.

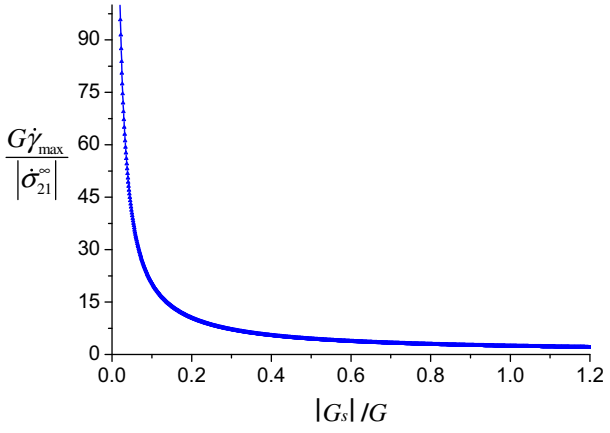

Fig. 5. The normalized maximum shear strain rate $G\dot{\gamma}_{max}/|\dot{\sigma}_{21}^{\infty}|$ versus the dimensionless softening secant modulus $|G_s|/G$.

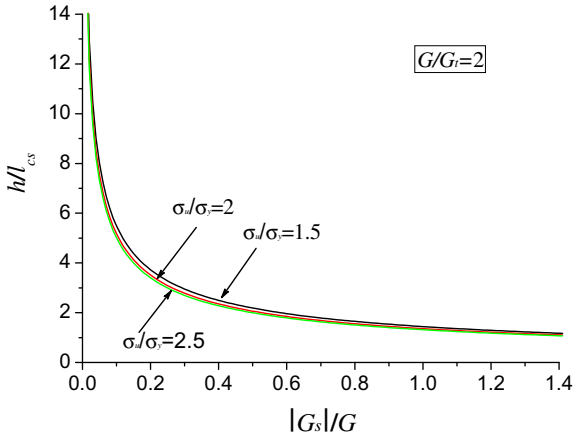

Fig. 6. The dimensionless thickness of shear band h/l_{cs} versus the dimensionless softening secant modulus $|G_s|/G$ for different ratios of the ultimate strength σ_u to the yield stress σ_y and $G_t = G/2$.

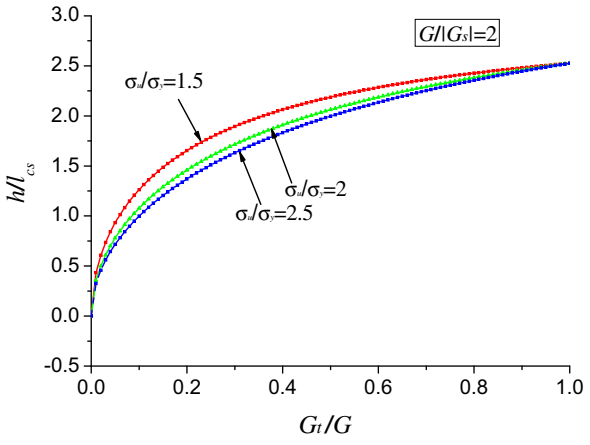

Fig. 7. The dimensionless thickness of shear band h/l_{cs} versus the dimensionless hardening secant modulus G_t/G for different ratios of the ultimate strength σ_u to the yield stress σ_y and $G_s = -G/2$.

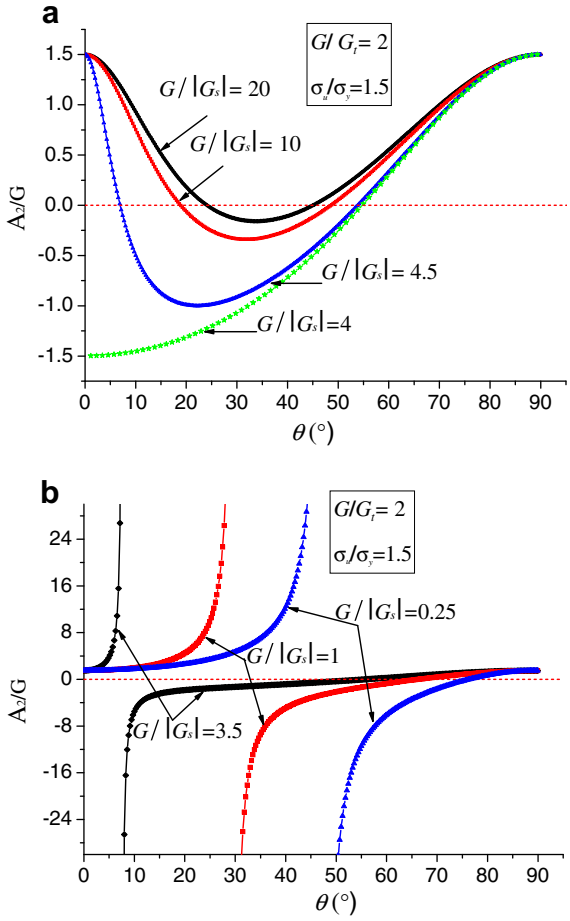

Fig. 8. The dimensionless parameter A_2/G versus the tilt angle θ of shear band for different ratios of elastic shear modulus G to the softening secant modulus $|G_s|$. The linear hardening secant modulus $G_t = G/2$ and the ratio of the ultimate strength σ_u to the yield stress σ_y is $\sigma_u/\sigma_y = 1.5$. (a) For $G/|G_s| \geqslant 4$; (b) for $G/|G_s| < 4$.

We assume that the linear hardening secant modulus $G_t = G/2$ and the ratio of the ultimate tensile strength σ_u to the yield stress σ_y is $\sigma_u/\sigma_y = 1.5$. When $G/|G_s|$ is approximately larger than 4, the dimensionless parameter A_2/G decreases first from 1.5 to a negative value and then increases to a positive value as shown in Fig. 8(a). It means there is an interval of θ to ensure a negative A_2 and shear band initiating. With the value $G/|G_s|$ decreasing, the interval ensuring $A_2 < 0$ increases, which means a larger softening secant modulus $|G_s|$ permits more chance and a much wider region for shear band initiating.

However, when the value $G/|G_s|$ is smaller than 4 or so, the variation trend of A_2/G is different from that in Fig. 8(a), which is shown in Fig. 8(b). For fixed material constants, the value A_2/G has a singular break at a critical angle θ. Smaller than the critical angle yields a positive A_2/G, which increases with an increasing θ. If θ is larger than the critical angle, A_2/G changes from a negative value to a positive one and there exists an interval ensuring A_2/G to be negative.

For a fixed value of $G/|G_s|$ and varying G/G_t, the relation between A_2/G and θ is found to be very similar to Fig. 8(a) and (b), but with an approximate value $G/G_t = 2$ to separate different varying trends like Fig. 8(a) and (b). The details are not repeated in the present paper.

Fig. 9(a) and (b) plot the relation between the dimensionless thickness of possible shear band h/l_{cs} and permitted tilt angle θ with fixed values $G/G_t = 2$ and $\sigma_u/\sigma_y = 1.5$ for cases of $G/|G_s| > 4$ and $G/|G_s| \leqslant 4$, respectively. From Fig. 9(a), one can see that the thickness of shear band decreases first and then almost keeps a constant, after that the value of thickness increases again, along with an increasing θ in its permitted region. The thickness of shear band tends to be very large near the smallest and largest permitted tilt angles, i.e., possible overall plastic flow may emerge, which is a hardly happening phenomenon for most materials. When $G/|G_s| \leqslant 4$, the dimensionless thickness of shear band keeps almost a constant in a wide region of the permitted tilt angles, then increases sharply near the largest permitted tilt angle.

The relation between the dimensionless thickness of shear band h/l_{cs} and permitted tilt angle θ with fixed values $G/|G_s|$ and σ_u/σ_y for different G/G_t is also very similar to that in Fig. 9(a) and (b), which is omitted here.

Fig. 10 plots the relation between the dimensionless thickness of shear band, h/l_{cs}, and the ratio $|G_s|/G$ for a fixed value of $G/G_t = 2$, a fixed tilt angle $\theta = \pi/5$ and different σ_u/σ_y. From Fig. 10, one can see that the dimensionless thickness of shear band decreases significantly with a decreasing value of $|G_s|/G$ for a determined σ_u/σ_y, and decreases slightly with an increasing σ_u/σ_y for a determined $|G_s|/G$.

Fig. 11 shows the dimensionless thickness of shear band, h/l_{cs}, as a function of the ratio G_t/G for a fixed value of $G/|G_s| = 4$, a fixed tilt

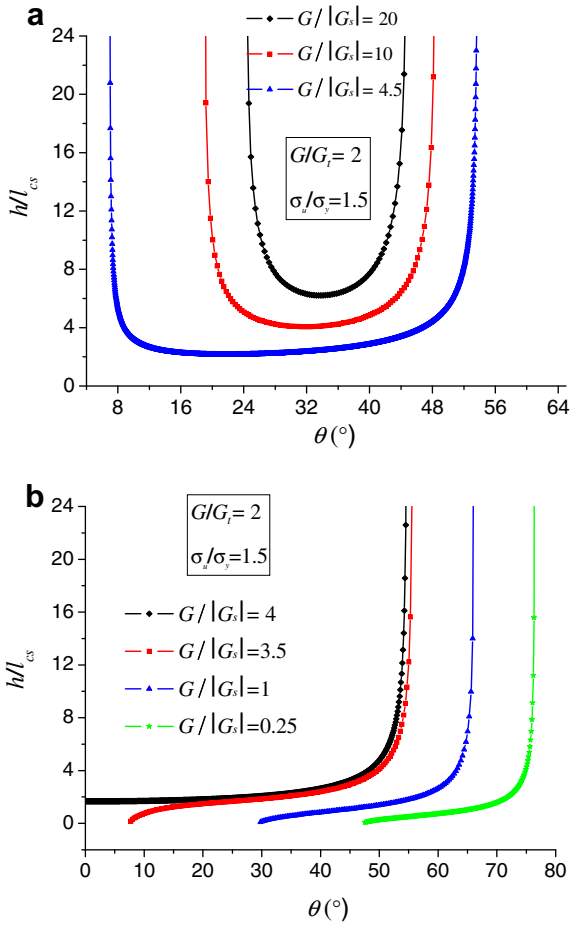

Fig. 9. The dimensionless thickness of shear band h/l_{cs} versus the tilt angle θ of shear band for different ratios of elastic shear modulus G to the softening secant modulus $|G_s|$. The linear hardening secant modulus $G_t = G/2$, the ratio of the ultimate strength σ_u to the yield stress σ_y is $\sigma_u/\sigma_y = 1.5$. (a) For $G/|G_s| \geqslant 4$; (b) for $G/|G_s| < 4$.

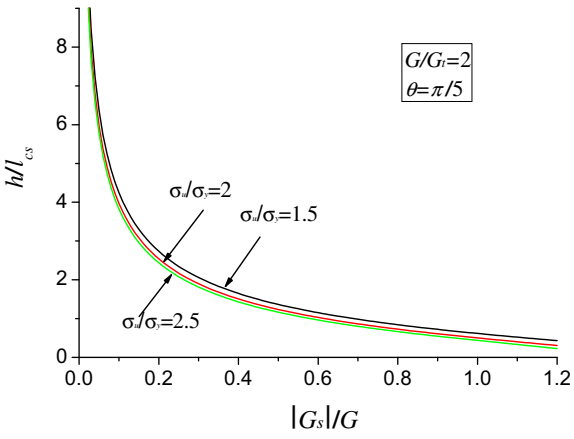

Fig. 10. The dimensionless thickness of shear band h/l_{cs} versus the dimensionless softening secant modulus $|G_s|/G$ for different ratios of the ultimate strength σ_u to the yield stress σ_y with $G/G_t = 2$ and $\theta = \pi/5$.

angle $\theta = \pi/5$ and different σ_u/σ_y. One can see that the dimensionless thickness of shear band increases from near zero to almost a constant 3 when G_t/G increases from zero to one for various σ_u/σ_y. The dimensionless thickness of shear band increases slightly when σ_u/σ_y decreases. Comparing Figs. 10 and 11 finds that the effect of $|G_s|/G$ on the dimensionless thickness is much more obvious than that of G_t/G.

In order to study the distribution of the generalized effective strain rate, we assume that the linear hardening secant modulus $G_t = G/2$; the softening secant modulus $G_s = -G/4$; the ratio of the ultimate strength σ_u and the yield stress σ_y is $\sigma_u/\sigma_y = 1.5$ and the tilt angle of shear band $\theta = \pi/5$. Fig. 12 shows the distribution of the generalized effective strain rate normalized by the remote shear strain rate, $3G\dot{E}_e/|\dot{\sigma}^\infty|$, inside and outside the shear band, where it is shown that the generalized effective strain rate inside the shear band increases monotonically from zero at the boundary of shear band to a maximum in the center. While the generalized effective strain rate is uniform a little outside the shear band. The non-uniformity of the generalized effective strain rate almost only exists inside and near the shear band. The maximum of the generalized effective strain rate is much larger than the remote one, which indicates clearly the plastic flow localization.

Fig. 13 shows the normalized maximum generalized effective strain rate $3G\dot{E}_{emax}/|\dot{\sigma}^\infty|$ versus the possible tilt angle θ with $G_s = -G/4$, $G_t = G/2$ and different ratio of ultimate tensile strength to the yield stress, σ_u/σ_y. The maximum generalized effective strain rate decreases with the increasing possible tilt angle, then keeps almost a constant in a small region of θ, after which the maximum generalized effective strain rate increases with the increasing possible tilt angle. The value of σ_u/σ_y does not show significant effect on $3G\dot{E}_{emax}/|\dot{\sigma}^\infty|$. It is interesting that one can infer from Fig. 13 that for a determined solid under uniaxial tension, the most possible tilt angle for the shear band initiating may correspond to the smallest value of $3G\dot{E}_{emax}/|\dot{\sigma}^\infty|$. For the solid studied in Fig. 13, the most possible tilt angle for the shear band initiating is about 37°.

Fig. 14 gives the relation of the normalized maximum generalized effective strain rate $3G\dot{E}_{emax}/|\dot{\sigma}^\infty|$ and the ratio of the linear hardening secant modulus to the shear modulus G_t/G for fixed values of $G_s = -G/4$, $\sigma_u/\sigma_y = 1.5$, and $\theta = \pi/5$. The maximum value of G_t/G is one. The normalized maximum generalized effective strain rate decreases sharply at the initial stage, then keeps almost a constant, when the value of G_t/G increases from zero to one.

Fig. 15 show the normalized maximum generalized effective strain rate $3G\dot{E}_{emax}/|\dot{\sigma}^\infty|$ versus the ratio of the softening secant modulus to the shear modulus $|G_s|/G$ for fixed values $G_t = G/2$, $\sigma_u/\sigma_y = 1.5$, and $\theta = \pi/5$. One can see that the normalized maximum generalized effective strain rate decreases sharply before $|G_s|/G = 0.1$, then decreases slowly for a wide range of $|G_s|/G$, after that the maximum generalized effective strain rate increases sharply

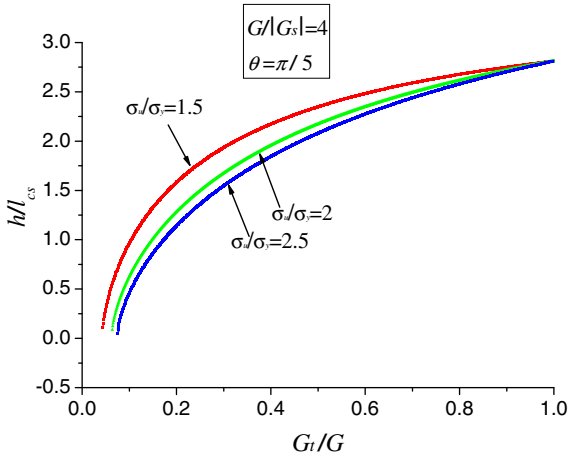

Fig. 11. The dimensionless thickness of shear band h/l_{cs} versus the dimensionless hardening secant modulus G_t/G for different ratios of the ultimate strength σ_u to the yield stress σ_y with $G/|G_s| = 4$ and $\theta = \pi/5$.

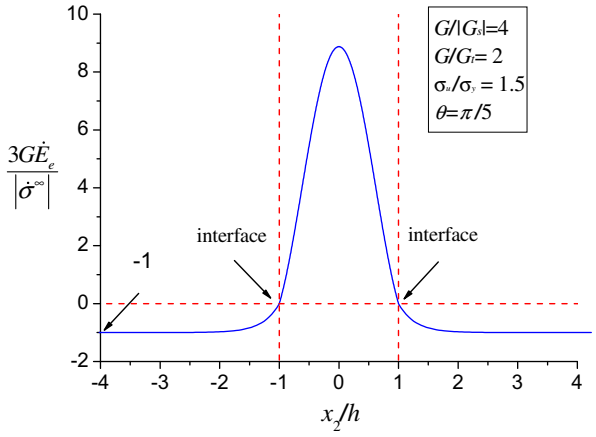

Fig. 12. The distribution of the normalized generalized effective strain rate $3G\dot{E}_e/|\dot{\sigma}^{\infty}|$ inside and outside the shear band, where $\dot{\sigma}^{\infty}$ is the remote tension stress rate and $G = 2G_t$, $G_s = -G/4$, $\theta = \pi/5$ and $\sigma_u/\sigma_y = 1.5$.

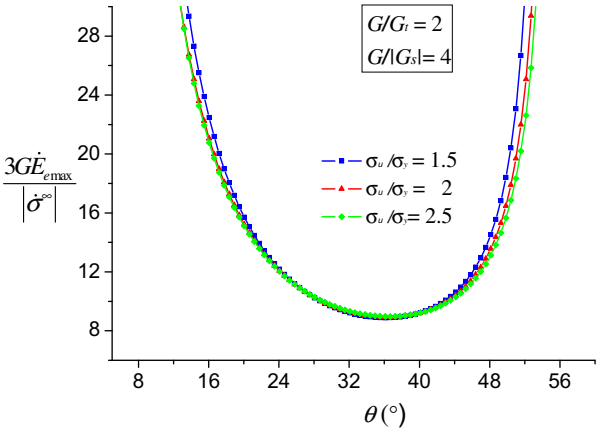

Fig. 13. The normalized maximum generalized effective strain rate $3G\dot{E}_{emax}/|\dot{\sigma}^{\infty}|$ versus the possible tilt angle of shear band θ with $G/|G_s| = 4$ and $G_t = G/2$.

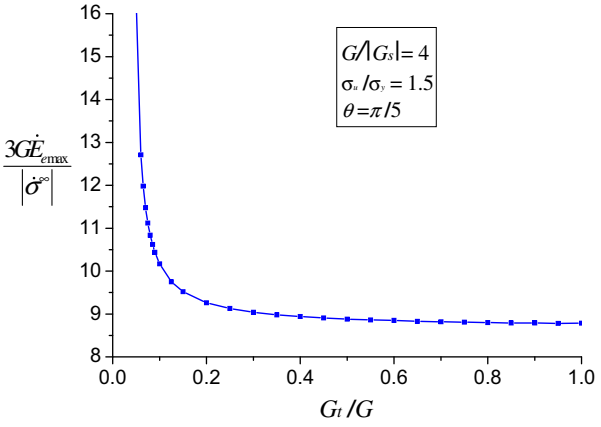

Fig. 14. The normalized maximum generalized effective strain rate $3G\dot{E}_{emax}/|\dot{\sigma}^{\infty}|$ versus the dimensionless hardening secant modulus G_t/G with $G/|G_s| = 4$, $\theta = \pi/5$ and $\sigma_u/\sigma_y = 1.5$.

when $|G_s|/G \geqslant 1.5$. The maximum generalized effective strain rate may achieve more than 20 times the remote strain rate, which also indicates clearly plastic flow localization.

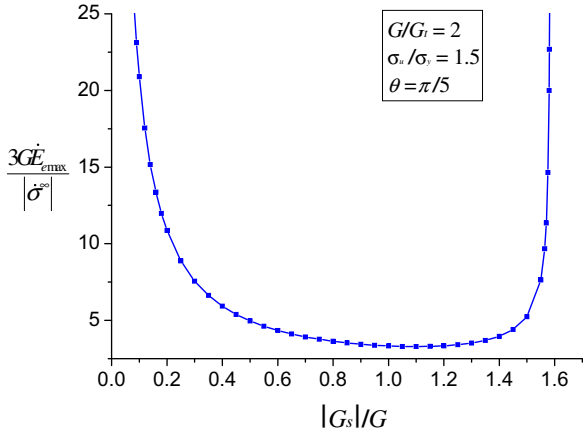

Fig. 15. The normalized maximum generalized effective strain rate $3G\dot{E}_{emax}/|\dot{\sigma}^{\infty}|$ versus the dimensionless softening secant modulus $|G_s|/G$ with $G_t = G/2$, $\theta = \pi/5$ and $\sigma_u/\sigma_y = 1.5$.

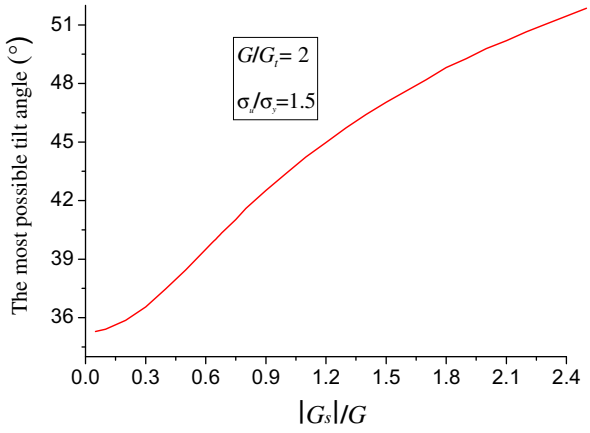

Fig. 16. The most possible tilt angle versus the dimensionless softening secant modulus $|G_s|/G$ with $G_t = G/2$ and $\sigma_u/\sigma_y = 1.5$.

6. Summary and discussion

Plastic flow localization in an infinite solid subjected to a pure shear loading and uniaxial tension is studied using a reduced strain gradient theory. The initial thickness of shear band in both cases can be obtained analytically.

The shear strain rate in the pure shear case and the generalized effective strain rate in the uniaxial tension case display an obvious non-uniformity inside and outside the shear band, which varies from zero at the boundary of shear band to a maximum in the center of the shear band. The maximum shear rate or the maximum generalized effective strain rate can achieve over tens times the remote uniform strain rate, which indicates significantly the plastic flow localization. The initial thickness of shear band is influenced more significantly by the softening secant modulus than the linear hardening secant one. The effect of ratio of the ultimate strength to the yield one on the shear band initial thickness is not very obvious.

Specially, in the uniaxial tension model, the most possible tilt angle for shear band initiating is the one, at which the maximum generalized effective strain rate attains the smallest value for all possible tilt angles as shown in Fig. 16, and is consistent qualitatively with experiment observations (Donovan, 1988; Donovan, 1989; Volkert et al., 2008).

The results in this paper should give some insights and guidance for engineers to predict the initial thickness of plastic flow localization and the most possible tilt angle of shear band initiating in a real metallic material.

Acknowledgments

The work reported here is supported by NSFC through Grants #10972220, #10732050, and #11021262. In addition, the authors should give their many thanks to the two anonymous reviewers for their helpful and professional suggestions.

References

Acharya, A., Beaudoin, A.J., 2000. Grain-size effect in viscoplastic polycrystals at moderate strains. J. Mech. Phys. Solids 48, 2213–2230.
Aifantis, E.C., 1984. On the microstructural origin of certain inelastic models. Trans. ASME J. Eng. Mater. Tech. 106, 326–330.
Aifantis, E.C., 1987. The physics of plastic deformation. Int. J. Plast. 3, 211–247.
Atkinson, M., 1995. Further analysis of the size effect in indentation hardness tests of some metals. J. Mater. Res. 10, 2908–2915.
Bassani, J.L., 2001. Incompatibility and a simple gradient theory of plasticity. J. Mech. Phys. Solids 49, 1983–1996.
Bassani, J.L., Acharya, A., 1995. Incompatible lattice deformations and crystal plasticity. Am. Soc. Mech. Eng., Appl. Mech. Div. 200, 75–80.
Chambon, R., Caillertie, D., Hassan, N.E., 1998. One-dimensional localization studied with a second grade model. Eur. J. Mech./A: Solids 17, 637–656.
Chen, S.H., Wang, T.C., 2000. A new hardening law for strain gradient plasticity. Acta Mater. 48, 3997–4005.
Chen, S.H., Wang, T.C., 2001. Strain gradient theory with couple stress for crystalline solids. Eur. J. Mech. A-Solids 20, 739–756.
Chen, S.H., Wang, T.C., 2002a. A new deformation theory with strain gradient effects. Int. J. Plast. 18, 971–995.
Chen, S.H., Wang, T.C., 2002b. Size effects in the particle-reinforced metal-matrix composites. Acta Mech. 157, 113–127.
Chen, S.H., Wang, T.C., 2002c. Finite element solutions for plane strain mode I crack with strain gradient effects. Int. J. Solids Struct. 39, 1241–1257.
Chen, S.H., Liu, L., Wang, T.C., 2004. Size dependent nanoindentation of a soft film on a hard substrate. Acta Mater. 52, 1089–1095.
Chen, S.H., Liu, L., Wang, T.C., 2005. Investigation of the mechanical properties of thin films by nano-indentation, considering the effects of thickness and different coating–substrate combinations. Surface Coatings Technol. 191, 25–32.
Cosserat, E., Cosserat, F., 1909. Theorie des Corps Deformables. Herman et fils, Paris.
De Borst, R., Van der Giessen, E., 1998. Material Instabilities in Solids. John Wiley & Sons, Chichester.
Donovan, P.E., 1988. Compressive deformation of amorphous Pd40ni40p20. Mater. Sci. Eng. 98, 487–490.
Donovan, P.E., 1989. A yield criterion for Pd40ni40p20 metallic-glass. Acta Metallurgica 37, 445–456.
Elssner, G., Korn, D., Ruhle, M., 1994. The influence of interface impurities on fracture energy of UHV diffusion-bonded metal–ceramic bicrystals. Scripta Metallurgica Et Materialia 31, 1037–1042.
Engelen, R.A.B., Geers, M.G.D., Baaijens, F.P.T., 1999. Gradient-enhanced plasticity formulations based on the dependency of the yield stress on a nonlocal field variable. In: Proceedings of European Conference on Computation Mechanics. Munich, Germany, on CD-ROM.
Engelen, R.A.B., Geers, M.G.D., Baaijens, F.P.T., 2003. Nonlocal implicit gradient-enhanced elasto-plasticity for the modeling of softening behavior. Int. J. Plasticity, 19 403–433.
Engelen, R.A.B., Fleck, N.a., Peerlings, R.H.J., Geers, M.G.D., 2006. An evaluation of higher-order plasticity theories for predicting size effects and localization. Int. J. Solids Struct. 43, 1857–1877.
Eringen, A.C., 1968. Theory of micropolar elasticity. In: Leibowitz, H. (Ed.), Fracture, An Advanced Treatise. Academic Press, New York, pp. 621–729.
Evers, L.P., Parks, D.M., Brekelmans, W.A.M., Geers, M.G.D., 2002. Crystal plasticity model with enhanced hardening by geometrically necessary dislocation accumulation. J. Mech. Phys. Solids 50, 2403–2424.
Feng, G., Nix, W.D., 2004. Indentation size effect in MgO. Scr. Mater. 51, 599–603.
Fleck, N.A., Hutchinson, J.W., 1993. A phenomenological theory for strain gradient effects in plasticity. J. Mech. Phys. Solids 41, 1825–1857.
Fleck, N.A., Hutchinson, J.W., 1997. Strain gradient plasticity. In: Hutchinson, J.W., Wu, T.Y. (Eds.), Advances in Applied Mechanics, vol. 33. Academic Press, New York, pp. 295–361.
Fleck, N.A., Hutchinson, J.W., 1998. A discussion of strain gradient plasticity theories and application to shear bands. In: The International Symposium on Material Instabilities in Solids, Netherlands, pp. 507–519.
Fleck, N.A., Hutchinson, J.W., 2001. A reformulation of strain gradient plasticity. J. Mech. Phys. Solids 49, 2245–2271.
Fleck, N.A., Willis, J.R., 2009. A mathematical basis for strain-gradient plasticity theory Part II: tensorial plastic multiplier. J. Mech. Phys. Solids 57, 1045–1057.
Fleck, N.A., Muller, G.M., Ashby, M.F., Hutchinson, J.W., 1994. Strain gradient plasticity theory and experiment. Acta Metallurgica Et Materialia 42, 475–487.
Gao, H.J., Huang, Y.G., 2001. Taylor-based nonlocal theory of plasticity. Int. J. Solids Struct. 38, 2615–2637.
Gao, H., Huang, Y., Nix, W.D., 1999a. Modeling plasticity at the micrometer scale. Naturwissenschaften 86, 507–515.
Gao, H., Huang, Y., Nix, W.D., Hutchinson, J.W., 1999b. Mechanism-based strain gradient plasticity-I theory. J. Mech. Phys. Solids 47, 1239–1263.
Gardiner, B.S., Tordesillas, A., 2004. Micromechanics of shear bands. Int. J. Solids Struct. 41, 5885–5901.
Gurtin, M.E., 2000. On the plasticity of single crystals: free energy, microforces, plastic-strain gradients. J. Mech. Phys. Solids 48, 989–1036.
Gurtin, M.E., 2002. A gradient theory of single-crystal viscoplasticity that accounts for geometrically necessary dislocations. J. Mech. Phys. Solids 50, 5–32.
Hadamad, J., 1903. Lecons sur la propagation des ondes et les équations de lÕhydrodynamique. Librarie Scientifique. A. Hermann, Paris.
Hill, R., 1958. A general theory of uniqueness and stability in elastic–plastic solids. J. Mech. Phys. Solids 6, 236–249.
Huang, Y., Gao, H., Nix, W.D., Hutchinson, J.W., 2000a. Mechanism-based strain gradient plasticity-II analysis. J. Mech. Phys. Solids 48, 99–128.
Huang, Y., Xue, Z., Gao, H., Nix, W.D., Xia, Z.C., 2000b. A study of microindentation hardness tests by mechanism-based strain gradient plasticity. J. Mater. Res. 15, 1786–1796.
Huang, Y., Qu, S., Hwang, K.C., Li, M., Gao, H., 2004. A conventional theory of mechanism-based strain gradient plasticity. Int. J. Plast. 20, 753–782.
Hu, G.K., Liu, X.N., Lu, T.J., 2005. A variational method for non-linear micropolar composites. Mech. Mater. 37, 407–425.
Hutchinson, J.W., 1997. Linking scales in fracture mechanics. In: Karihaloo, B.L., Mai, Y.W., Ripley, M.I., Ritchie, R.O. (Eds.), Advances in Fracture Research. Pergamon Press, New York, pp. 1–14.
Hwang, K.C., Jiang, H., Huang, Y., Gao, H., Hu, N., 2002. A finite deformation theory of strain gradient plasticity. J. Mech. Phys. Solids 50, 81–99.
Hwang, K.C., Jiang, H., Huang, Y., Gao, H., 2003. Finite deformation analysis of mechanism-based strain gradient plasticity: torsion and crack tip field. Int. J. Plast. 19, 235–251.
Jiang, H., Huang, Y., Zhuang, Z., Hwang, K.C., 2001. Fracture in mechanism-based strain gradient plasticity. J. Mech. Phys. Solids 49, 979–993.
Jirasek, M., Rolshoven, S., 2009a. Localization properties of strain-softening gradient plasticity models Part I: strain-gradient theories. Int. J. Solids Struct. 46, 2225–2238.
Jirasek, M., Rolshoven, S., 2009b. Localization properties of strain-softening gradient plasticity models. Part II: theories with gradients of internal variables. Int. J. Solids Struct. 46, 2239–2254.
Lam, D.C.C., Yang, F., Chong, A.C.M., Wang, J., Tong, P., 2003. Experiments and theory in strain gradient elasticity. J. Mech. Phys. Solids 51, 1477–1508.
Liu, X., Hu, G., 2005. A continuum micromechanical theory of overall plasticity for particulate composites including particle size effect. Int. J. Plasticity 21, 777–799.
Lloyd, D.J., 1994. Particle reinforced aluminum and magnesium matrix composites. Int. Mater. Rev. 39, 1–23.
Ma, Q., Clarke, D.R., 1995. Size-dependent hardness of silver single-crystals. J. Mater. Res. 10, 853–863.
McElhaney, K.W., Vlassak, J.J., Nix, W.D., 1998. Determination of indenter tip geometry and indentation contact area for depth-sensing indentation experiments. J. Mater. Res. 13, 1300–1306.
Mikkelsen, L.P., Goutianos, S., 2009. Suppressed plastic deformation at blunt crack-tips due to strain gradient effects. Int. J. Solids Struct. 46, 4430–4436.
Mindlin, R.D., 1964. Micro-structure in linear elasticity. Arch. Ration. Mech. Anal. 16, 51–78.
Mindlin, R.D., 1965. Second gradient of strain and surface tension in linear elasticity. Int. J. Solids Struct. 1, 417–438.
Nix, W.D., Gao, H.J., 1998. Indentation size effects in crystalline materials: a law for strain gradient plasticity. J. Mech. Phys. Solids 46, 411–425.
Oda, M., Iwashita, K., 2000. Study on couple stress and shear band development in granular media based on numerical simulation analyses. Int. J. Eng. Sci. 38, 1713–1740.
Oda, M., Kazama, H., 1998. Microstructure of shear bands and its relation to the mechanisms of dilatency and failure of dense granular soils. Geotechnique 48, 465–481.
Oda, M., Konishi, J., Nemat-Nasser, S., 1982. Experimental micromechanical evaluation of the strength of granular materials: effects of particle rolling. Mech. Mater. 1, 269–283.
Ortiz, M., 1987. An analytical study of the localized failure modes of concrete. Mech. Mater. 6, 159–174.
Osinov, V.A., Wu, W., 2009. Strain-gradient extension of hypoplasticity. Acta Mech. 203, 37–47.
Ottosen, N.E., Runesson, K., 1991. Properties of discontinuous bifurcation solutions in elasto-plasticity. Int. J. Solids Struct. 27, 401–421.
Peirce, D., Asaro, R.J., Needleman, A., 1983. Material rate dependence and localized deformation in crystalline solids. Acta Metall. 31, 1951–1976.
Rice, J.R., 1976. The localization of plastic deformation. In: Koiter, W.T. (Ed.), Theoretical and Applied Mechanics, vol. 1. North-Holland Publishing Company, pp. 207–220.
Rudnicki, J.W., Rice, J.R., 1975. Conditions for the localization of deformation in pressure-sensitive dilatant materials. J. Mech. Phys. Solids 23, 371–395.

Saha, R., Nix, W.D., 2002. Effects of the substrate on the determination of thin film mechanical properties by nanoindentation. Acta Mater. 50, 23–38.
Saha, R., Xue, Z.Y., Huang, Y., Nix, W.D., 2001. Indentation of a soft metal film on a hard substrate: strain gradient hardening effects. J. Mech. Phys. Solids 49, 1997–2014.
Schuster, B.E., Wei, Q., Ervin, M.H., Hruszkewycz, S.O., Miller, M.K., Hufnagel, T.C., Ramesh, K.T., 2007. Bulk and microscale compressive properties of a Pd-based metallic glass. Scr. Mater. 57, 517–520.
Schuster, B.E., Wei, Q., Hufnagel, T.C., Ramesh, K.T., 2008. Size-independent strength and deformation mode in compression of a Pd-based metallic glass. Acta Mater. 56, 5091–5100.
Shi, M.X., Huang, Y., Hwang, K.C., 2000. Plastic flow localization in mechanism-based strain gradient plasticity. Int. J. Mech. Sci. 42, 2115–2131.
Shi, Z., Huang, Y., Song, J., Hwang, K.C., Li, M., 2009. Study of plastic shear localization via the flow theory of mechanism-based strain gradient plasticity. J. Eng. Mech.–ASCE 135, 132–138.
Shu, J.Y., Fleck, N.A., 1999. Strain gradient crystal plasticity: size-dependent deformation of bicrystals. J. Mech. Phys. Solids 47, 297–324.
Smyshlyaev, V.P., Fleck, N.A., 1996. The role of strain gradients in the grain size effect for polycrystals. J. Mech. Phys. Solids 44, 465–495.
Stelmashenko, N.A., Walls, M.G., Brown, L.M., Milman, Y.V., 1993. Microindentations on W and Mo oriented single crystals: an STM study. Acta Metallurgica Et Materialia 41, 2855–2865.
Stolken, J.S., Evans, A.G., 1998. A microbend test method for measuring the plasticity length scale. Acta Mater. 46, 5109–5115.
Swadener, J.G., George, E.P., Pharr, G.M., 2002. The correlation of the indentation size effect measured with indenters of various shapes. J. Mech. Phys. Solids 50, 681–694.
Thomas, T., 1961. Plastic Flow and Fracture in Solids. Academic Press, New York.
Toupin, R., 1962. Elastic materials with couple-stresses. Arch. Rat. Mech. Anal. 11, 385–414.
Volkert, C.A., Donohue, A., Spaepen, F., 2008. Effect of sample size on deformation in amorphous metals. J. Appl. Phys. 103, 083539.
Wei, Y., 2001. Particulate size effects in the particle-reinforced metal-matrix composites. Acta Mech. Sin. 17, 45–58.
Wei, Y., Hutchinson, J.W., 1997. Steady-state crack growth and work of fracture for solids characterized by strain gradient plasticity. J. Mech. Phys. Solids 45, 1253–1273.
Wei, Y., Hutchinson, J.W., 2003. Hardness trends in micro scale indentation. J. Mech. Phys. Solids 51, 2037–2056.
Xue, Z., Huang, Y., Hwang, K.C., Li, M., 2002. The influence of indenter tip radius on the micro-indentation hardness. J. Eng. Mater. Tech. 124, 371–379.
Yang, J., Cady, C., Hu, M.S., Zok, F., Mehrabian, R., Evans, A.G., 1990. Effects of damage of the flow strength and ductility of a ductile Al-alloy reinforced with SiC particulates. Acta Metallurgica Et Materialia 38, 2613–2619.
Yang, F., Chong, A.C.M., Lam, D.C.C., Tong, P., 2002. Couple stress based strain gradient theory for elasticity. Int. J. Solids Struct. 39, 2731–2743.
Yi, D.K., Wang, T.C., Chen, S.H., 2009. New strain gradient theory and analysis. Acta Mech. Solida Sin. 22, 45–52.
Zbib, H.M., Aifantis, E.C., 1988. On the structure and width of shear bands. Scr. Met. 22, 703–708.
Zbib, H.M., Aifantis, E.C., 1992. On the gradient-dependent theory of plasticity and shear banding. Acta Mech. 92, 209–225.
Zhao, J.D., Sheng, D.C., Zhou, W.Y., 2005. Shear banding analysis of geomaterials by strain gradient enhanced damage model. Int. J. Solids Struct. 42, 5335–5355.